Available at: http://publications.ictp.it IC/2010/002

United Nations Educational, Scientific and Cultural Organization
and
International Atomic Energy Agency
THE ABDUS SALAM INTERNATIONAL CENTRE FOR THEORETICAL PHYSICS

CARBON IN PALLADIUM CATALYSTS: A METASTABLE CARBIDE

Nicola Seriani[1]
Fakultät für Physik, Universität Wien, Sensengasse 8, A-1090 Wien, Austria
and
The Abdus Salam International Centre for Theoretical Physics, Trieste, Italy

Florian Mittendorfer and Georg Kresse
Fakultät für Physik, Universität Wien, Sensengasse 8, A-1090 Wien, Austria.

Abstract

The catalytic activity of palladium towards selective hydrogenation of hydrocarbons depends on the partial pressure of hydrogen. It has been suggested that the reaction proceeds selectively towards partial hydrogenation only when a carbon-rich film is present at the metal surface. On the basis of first-principles simulations, we show that carbon can dissolve into the metal because graphite formation is delayed by the large critical nucleus necessary for graphite nucleation. A bulk carbide Pd_6C with a hexagonal 6-layer fcc-like supercell forms. The structure is characterized by core level shifts of 0.66-0.70 eV in the core states of Pd, in agreement with experimental x-ray photoemission spectra. Moreover, this phase traps bulk-dissolved hydrogen, suppressing the total hydrogenation reaction channel and fostering partial hydrogenation.

MIRAMARE – TRIESTE
January 2010

[1] nseriani@ictp.it

1 Introduction

Partial hydrogenation reactions play a fundamental role in the chemical industry. Polyethylene production by homogenous catalysis requires the previous purification of the ethene (ethylene) feed through partial hydrogenation of highly unsaturated hydrocarbons such as ethyne (acetylene) [1–6], which would otherwise poison the homogenous catalyst involved in ethylene polymerization [7, 8]. The partial hydrogenation reaction of ethyne to ethylene is catalyzed heterogeneously by catalysts based on palladium nanoparticles, sometimes doped with lead [9, 10], silver [4] or other metals [3].

Selectivity of palladium towards the product ethylene is highly dependent on the ratio of the partial pressures of hydrogen and ethyne. On a palladium catalyst at high hydrogen pressures, the complete hydrogenation to ethane prevails, whereas lower hydrogen pressure favours a higher selectivity towards ethylene, with selectivity nearly reaching 100% [11]. Recently it has been suggested that the key to the high selectivity at low hydrogen pressure is the formation of a 1.4 nanometer thick carbon-rich phase on the surface of the metal [11,12]. A fingerprint of this phase is a shift of 0.6 eV in the 3d peak of the x-ray photoelectron spectrum (XPS) of palladium. Recently, the same authors proposed that this might be due to dissolved carbon at the surface [13]. On the other hand, a large variety of mixed phases are known to form on palladium nanoparticles exposed to a hydrocarbon-rich atmosphere; collectively, these phases are known as coke [14–18]. They might be harmful or harmless, 'invisible' or beneficial for the reaction of partial hydrogenation [14,15], depending on their exact nature. In these phases, palladium might exist in a variety of chemical states, as seen in the shifts of the electronic core levels of Pd [19]. Depending on conditions and on history of the catalyst, these species may comprise graphite, amorphous carbon with sp^3 hybridization, and green oil (long-chained hydrocarbons) [15–18, 20].

Questions about the stability of carbon species, their formation pathways and their role in the hydrogenation catalysis and in catalyst deactivation are largely unanswered. In particular, it is unclear why Pd-C phases should form instead of graphite layers on the surface. In the present work, we have consequently investigated the thermodynamic stability and formation of possible Pd-C phases by means of density functional theory. For a direct comparison with the experimental findings, we have calculated the core level shifts of the relevant Pd-C phases, as well as of selected systems containing hydrogen. In the following section we briefly introduce the computational methods employed, then the results are reported and the conclusions are drawn. A summary concludes the article.

2 Computational methods

Simulations have been performed within density functional theory (DFT) in the generalized gradient approximation of Perdew, Burke, and Ernzerhof (PBE) [21]. Electronic wavefunctions have been described by the projector-augmented wave method (PAW) of Blöchl [22, 23] implemented

in the plane-wave code VASP [24]. The selfconsistent procedure for the electronic degrees of freedom was considered converged when the difference in total energy and the difference in the sum of the eigenvalues between two subsequent steps were both smaller than 10^{-4} eV. Structural relaxations have been performed until the absolute forces on each of the atoms were smaller than 0.02 eV/Å. In the optimized bulk structures the pressure was lower than 0.5 kbar. A cutoff of 275 eV has been employed; for the Pd_6C phase, structural optimization with a cutoff of 400 eV results in differences in the lattice constant smaller than 0.01 Å. For the same structure, a Monkhorst-Pack grid of (8×8×2) k-points was employed. Structural optimization with an increased grid of (12×12×4) results again in variations of the lattice constant smaller than 0.01 Å. For the (2×2) cell of the Pd(100) surface, a (8×8×1) mesh of k-points has been employed. The Pd(100) surface has been modeled with a slab with 6 Pd layers and has been fully relaxed. It has been checked that adsorption energies differ by less than 10 meV from those calculated with a slab with 8 layers. Adsorption systems have been simulated with an asymmetic model, i.e. with the adsorbate only on one side of the slab. Core level shifts have been calculated in the final state approximation by the method presented in Ref. [25]. Energy barriers have been calculated by constrained dynamics and the nudged-elastic band (NEB) method [26] with up to 5 images.

3 Results

The results are organized in five sections: 1) investigation of hydrocarbon adsorption; 2) discussion of the formation of the Pd_6C bulk carbide, 3) investigation of initial stages of carbon incorporation, 4) study of graphite formation at the surface within classical nucleation theory; and finally 5) the effect of Pd_6C formation on bulk diffusion of hydrogen and the adsorption of hydrocarbons.

3.1 Adsorption of hydrocarbons

Palladium catalysts are commonly used for hydrogenation reactions. As a first step in the investigation of the catalytic process, we focused on the adsorption of ethyne on low-index palladium surfaces Pd(111) and Pd(100). First, it is important to realise that ethyne is only a metastable compound, as shown by the DFT-GGA formation energy of 1.04 eV/C atom with respect to graphite and molecular hydrogen. For comparison, ethene (ethylene) has a formation energy of −0.09 eV, and ethane of −0.97 eV. The adsorption energies of ethyne and its fragments on Pd(111) and Pd(100) are reported in Tab. 1. Ethyne adsorbs on Pd(111) in a threefold hollow site [27–29] with an adsorption energy of −2.04 eV. On Pd(100) a fourfold-hollow site is more favorable, with an adsorption energy of −2.75 eV (Fig. 1), analogously to Cu(100) [30], whereas adsorption on a bridge position on Pd(100) leads to an adsorption energy of −1.59 eV. The energies are calculated with respect to an isolated ethyne molecule in the gas phase and the bare surface. Despite the strong interaction between hydrogen and palladium, a full dehydrogenation of ethyne to a carbon dimer on the surface and two co-adsorbed hydrogen atoms at the surface

is rather unfavourable and costs 1.67 eV on Pd(111), and 1.38 eV on Pd(100). An energetically more favourable reaction involves the breaking of the triple C-C bond, leading to the dissociation of the ethyne into two CH species. Yet also this step is endothermic with an energy cost of 0.32 eV on Pd(111). Further decomposition into adsorbed C and H is again endothermic by further 0.14 eV/C atom. The situation changes going to the more open Pd(100) surface. The dissociation of the ethyne into two CH species adsorbed in fourfold hollow sites on Pd(100) leads to an energy gain of 0.06 eV with respect to the adsorbed ethyne. Further decomposition of one CH species into adsorbed C and H leads to a further energy gain of 0.4 eV/C atom. Thus there is a strong thermodynamic driving force towards complete ethyne dissociation on a clean Pd(100) surface, but not on Pd(111). We conclude that atomic carbon and hydrogen are present on a real catalyst under operating conditions, whereas a different behaviour is expected on a single-crystal Pd(111) surface.

3.2 Stability of bulk phases

3.2.1 Bulk carbides

The presence of both hydrogen and carbon at the surface raises the question of the incorporation of the adsorbates into the substrate. The two species display quite different properties: while dissolved carbon is only metastable with respect to graphite (see next section), the incorporation of hydrogen leads to the formation of stable hydrides. The most stable bulk carbide that we found has a Pd_6C stoichiometry. The structure consists of the fcc lattice of palladium with a 3% expansion with a regular arrangement of C atoms in the octahedral sites (Fig. 2). The elementary cell has 6 Pd layers along the (111) direction of fcc Pd and a $(\sqrt{3} \times \sqrt{3})$ periodicity in the hexagonal plane perpendicular to this direction. The structure can be also built by arranging Pd_6C octahedra in a space-filling manner, such that each Pd atom is coordinated to a single C atom. The d-band center of this compound is -2.51 eV, lower than for metallic Pd (-2.20 eV). According to the d-band model [31], this should imply a decreased reactivity, and thus a stronger tendency towards partial hydrogenation. The formation energy of this phase is slightly endothermic 0.23 eV/C atom with respect to bulk Pd and graphite. Remarkably, other structures based on carbon dissolved in the fcc lattice of palladium with lower or higher C content yield less favourable formation energies. To model low concentrations, a cubic supercell with 32 Pd atoms was used. For one C atom a formation energy of 0.92 eV, and for two C atoms a formation energy of 0.77 eV/C atom was found (Tab. 2). At high concentrations, however, for one carbon atom in the conventional fcc Pd cell (4 Pd atoms), we also obtain a very unfavourable formation energy of 1.16 eV.

Notably, the Pd_6C phase has a 14 at% carbon content, matching the value of 13% measured upon carburization of Pd [32–35]. Moreover, the core level shifts of the 3d states of palladium are 0.66-0.70 eV, in agreement with the values measured in a Pd catalyst under reaction conditions [11, 12]. As already elaborated above, in this phase, the Pd lattice is expanded by 3% with

respect to the pure metal, slightly less than the 5% lattice expansion observed by High-Resolution Transmission Electron Microscopy (HRTEM) in the surface region of the Pd catalyst under operating conditions [12].

Although this phase agrees with the experimental data available, a careful search for other possible palladium carbide structures has been performed. In this section, we show that the other possible candidates have a less favourable formation energy, and that their CLS are incompatible with the experimental spectra. We have conducted a structural search for possible candidates of bulk palladium carbides by calculating the structures of known carbides of transition metals and by performing a less restricted search using genetic algorithms. As possible bulk Pd-C phases, we have considered the hexagonal crystal structure of bulk Pd_2C proposed in Ref. [36], and the crystal structures of carbides of transition metals reported in the literature (Tab. 2). The relaxation of the structure proposed in Ref. [36] leads to a drastic expansion of the volume, and the high formation energy of 4.4 eV/C atom rules out this particular model. The other crystal structures considered are those of the carbides Sc_2C, Ti_2C, Cr_3C_2, $Cr_{23}C_6$, Mn_5C_2, Mn_7C_3, Fe_2C, Fe_3C, Co_2C, Co_3C, Ni_3C, Y_2C, Nb_2C, Mo_2C, W_2C, Ta_2C, PtC (rocksalt [37]), PtN (zincblende [38]) and rutile. For some structures, namely the rutile, Mo_2C-based and Ni_3C-based structures, the relaxed models consist of carbon in octahedral sites of a distorted fcc lattice of Pd atoms. The formation energies of 1.19 eV/C atom (rutile and Mo_2C-based) and 1.20 eV/C atom (Ni_3C-based) are rather close to the value of 1.16 eV/C atom for the model with one carbon atom in an octahedral site in the conventional cell of metallic Pd (Pd_4C), but considerably higher than for the optimal Pd_6C structure. This is probably due to the fact that, contrary to Pd_6C, in these structures some Pd atoms are coordinated to more than one C atom. Also the calculated core level shifts of these potential carbide phases yield an unambiguous message: the bulk phases reported here yield core level shifts of 1.4 eV to 2 eV for the Pd atoms, in strong contrast to the value of 0.6 eV measured for the active film. In particular, for the rocksalt structure CLS of 2 eV have been found; the carbon-poor Mn_7C_3 yields smaller CLS of 1.4-1.5 eV.

To confirm these results, we have also performed a structural search using a genetic optimization algorithm similar to that used by Oganov et al. [39] and Trimarchi et al. [40]. The algorithm was applied with the simulation cell kept fixed at the configuration found upon relaxation of the hexagonal structure. Each run of the genetic algorithm started with the production of a population of 10-14 structures with carbon and palladium atoms put at random initial positions in the simulation cell. At each step of the run, the structures were fully relaxed by ab-initio damped molecular dynamics. Each structure was then 'coupled' to another one ('parents'), and one slice of the cell was exchanged between the two structures. In this way two new structures ('children') were produced and then relaxed. Atoms could be removed, added or exchanged with atoms of a different species with a predefined probability. The structure with the lowest free energy among the first parent and the children survived, the others were discarded. Once the algorithm was converged to one structure, this was put in a blacklist to force the population away from it in

subsequent runs. During population evolution the number of atoms, stoichiometry, local coordination and fractional coordinates of atoms were allowed to vary. After ∼200 generations, the best structures contained only single carbon atoms occupying octahedral sites in a distorted fcc Pd metal. We are thus confident that no other possible structure has been overlooked in this supercell.

Summarizing, a Pd_6C phase yields the lowest formation energy of 0.23 eV/C atom for a bulk carbide phase, and its CLS are 0.66-0.70 eV, compatible with the experimentally observed spectra. Still, the formation of this phase is endothermic, i.e. graphite formation is thermodynamically favored.

3.2.2 Bulk hydrides

In contrast to carbon, it is much easier to incorporate hydrogen into palladium. If the hydrogen pressure is sufficiently high, a palladium hydride is the stable bulk phase. Inserting up to 4 H atoms in a cubic cell of metallic Pd with 4 Pd atoms and allowing for optimization of the atomic positions and of the lattice parameters, our finding is that the system with 3 H atoms in octahedral sites has the lowest formation energy (−0.20 eV/H atom), but with a formation energy of −0.15 eV/H atom 4 H atoms per cell are only slightly less stable. The system with 3 (4) H atoms has a lattice expansion of 3.6% (4.5%), slightly lower than the 5% lattice expansion measured in experiment [12].

3.3 Initial stages of carbon incorporation

In the previous section we have shown that carbon incorporation into Pd and Pd_6C formation are endothermic with respect to graphite formation. Evidently, the experimentally observed carbon incorporation into the metal must be the result of the interplay of thermodynamic and kinetic effects during the carbon deposition. To understand these, the energetics of the deposition of carbon on and below the surface has been investigated. Different amounts of carbon at the surface or in the near-surface region have been simulated, in a $(\sqrt{3} \times \sqrt{3})$ surface cell of Pd(111), and in a (2×2) surface cell of Pd(100). On the less reactive Pd(111), carbon adsorption is endothermic in any position (Tab. 3). In agreement with a recent publication [13], we find that a single carbon atom prefers to be located in a subsurface octahedral position (E_{ads}=0.18 eV, Fig. 3(a)) rather than on the surface (E_{ads}=0.93 eV), with an energy difference of 0.75 eV. Thus, after a C atom has dissolved into the metal, there is a strong tendency for it to remain there. With two C atoms in the simulation cell, the most favored system has one C atom in a subsurface octahedral position and the other one two layers below (*1sub1subsubsub*), with a formation energy of 0.27 eV/C atom with respect to the bare Pd surface and graphite. This system has essentially the same atomic configuration and formation energy as bulk Pd_6C.

On the more open Pd(100) surface, a carbon atom adsorbes in the fourfold hollow site at the surface with an adsorption energy of −0.25 eV (Fig. 3(c)). This is the only Pd-C structure for

which we have found an exothermic energy of formation with respect to graphite. At variance to Pd(111), on this facet the surface position is the most stable one at low carbon coverage. However, the situation changes when the carbon content is increased. Already a second carbon in the (2×2) simulation cell prefers to go into the metal, with a position two layers below the surface (Fig. 3(d)) more favorable than a subsurface position, in analogy to the structure of Pd_6C (see the previous section and Fig. 2). These results suggest that, at intermediate carbon coverage ($\geq$1/2 ML), carbon dissolution into the metal is again preferred. With three carbon atoms in the simulation cell, carbon occupies the surface site, an octahedral site in a subsurface position and a site two layers below the surface, resulting in a thin film ∼6 Å thick with ∼20 at% carbon (Fig. 3(e)).

As in the case of bulk Pd_6C, also in these surface systems a low amount of dissolved carbon yields core level shifts of Pd in agreement with those measured. We have calculated the CLS for the two most stable systems with carbon on Pd(111) (Tab. 4), namely with one C atom in a subsurface position (*1sub*, Fig. 3(a)) and with a second C atom two layers below (*1sub1subsubsub*, Fig. 3(b)). The system with only one carbon in a subsurface position yields a CLS of ∼0.5 eV for the surface Pd layer and ∼0.6 eV in the subsurface layer. In the deeper layers the CLS are negligible. Thus, a single C atom induces a CLS of roughly 0.6 eV in its first Pd coordination shell, in perfect agreement with the experimentally observed peak. Similar CLS are found in the *1sub1subsubsub* system (Tab. 4).

For Pd(100) we have calculated the CLS with dissolved carbon and/or hydrogen (Tab. 5 and Tab. 6). For dissolved carbon, two systems have been considered: the most favorable system with 2 carbon atoms (*1surf1subsub*), with one C atom at the surface and one C atom 2 layers below (∼14% C content in the topmost three layers, Fig. 3(d)), similarly to Pd_6C, and the system with three C atoms (*1surf1sub1subsub*, Fig. 3(e)). In the system with 2 C atoms, the surface Pd atoms have a CLS of 0.49 eV. In the subsurface layer, the four Pd atoms have shifts of 0.57, 0.71, −0.25 and −0.25 eV, depending on their relative position to the C atoms. In the third layer, the CLS are 0.75 eV. Thus this system yields CLS very similar to those found experimentally. On the contrary, the system with three C atoms (20% C content in the topmost three layers) has too large CLS, in the range of 0.6-1.1 eV (Tab. 5). Notably, the CLS of a Pd atom can be brought in relation with its carbon coordination: two surface Pd atoms with CLS of 0.62 eV have one C atom at a distance less than 2.5 Å, with the second nearest C atom at 3.45 Å (type I). The Pd atom with a CLS of 0.73 eV has also only one C atom at a distance less than 2.5 Å, but the second nearest lies 4.32-4.40 Å away (type II). The fourth Pd atom has a CLS of 1.02 eV and lies directly above the carbon in the subsurface site, and thus has two carbon atoms at a distance less than 2.5 Å (type III). The same rules apply to Pd atoms in the lower layers, but with different values of the CLS: 0.74-0.79 eV for type I, 0.91-0.93 for type II, and 1.10-1.15 for type III. The presence of the C atom in a neighbourhood of the palladium atom influences the electronic structure of the metal atom. Baraldi et al. [41] have proposed a concept of effective coordination to quantify this

effect, and have shown that the core level shifts are a linear function of the effective coordination. In analogy to their work, we have calculated the effective Pd-C coordination of a Pd atom as a sum over the neighbouring C atoms of the Pd atoms $n_{eff}=\sum_i \exp(-b \cdot r_{ij})$, where r_{ij} is the Pd-C distance and b is the decay constant of the charge of the isolated atom. For b we have taken a value of 3.0719 $Å^{-1}$ [42]. For the Pd(100) surface with three C atoms (*1surf1sub1subsub*), we find that the core level shifts display a linear dependence on the effective coordination with a correlation coefficient of 0.92 (probability $< 0.1\%$). This analysis of the CLS of Pd atoms in surface models with different carbon content and configurations confirms the results reported in the section on bulk carbides: to obtain CLS near to the experimental value of 0.6 eV, a Pd atom has to have only one C atom in its direct neighbourhood, as it is the case for bulk Pd_6C, which consists of non-overlapping Pd_6-octahedra with a single C atom in the octahedral site.
To gain insight on the effect of hydrogen on the initial carbon dissolution into the metal, a hydrogen-rich Pd(100) surface has been investigated (Fig. 3(f)). This model consists of 6 H atoms, 2 per layer starting from the surface. In the absence of carbon, the formation energy is -0.28 eV/H atom. Addition of one carbon atom at the surface is still exothermic (-0.06 eV/C atom), as on the hydrogen-free surface, and the addition of a further C atom in the subsub position gives an overall C adsorption energy of 0.53 eV/C atom. Thus the trend in adsorption energy for carbon adsorption and dissolution is similar on the surfaces with and without hydrogen, with the C incorporation process being more favorable on the H-free surface. The effect of hydrogen is to raise the CLS of palladium with respect to the relative carbon-only system. Since dissolved hydrogen alone gives CLS lower than 0.4 eV (Tab. 5), it cannot explain the observed spectrum.

3.4 Suppression of graphite nucleation at the surface

Pd_6C and the surface systems with dissolved carbon have an endothermic energy of formation with respect to graphite. Yet the carbon dissolution into the metal can be more facile than graphite nucleation at the surface, as it can be shown by classical nucleation theory. In classical nucleation theory, the total energy of a graphene patch with radius r at the surface is given by

$$E(r) = \Delta H * N_C + E_{edge} * P, \tag{1}$$

where ΔH is the energy difference between a carbon atom dissolved in the metal and a carbon atom in an infinite graphene layer adsorbed at the surface, N_C is the number of carbon atoms in the graphene patch, E_{edge} is the edge energy for the graphene edge and P is the perimeter of the graphene patch. The critical radius for the island growth is determined by the competition between the energy gain for graphene formation and the cost for the formation of the edges. In the following we give an estimate of this critical radius for the formation of adsorbed graphene, assuming that the carbon originates from a dissolved state. In particular, we have considered the Pd(100) surface, where Pd-C interaction is expected to be stronger and therefore to lower the edge energy of the graphene patches by a larger amount. The adsorption energy of a graphene layer has

been calculated in a (6×3) cell. In absence of experimental information on the atomistic structure of the graphene/Pd(100) system, this surface cell has been chosen because it minimizes the strain of the graphene. Indeed, with the graphene oriented to have C-C bonds in the direction of the shorter surface cell vector, graphene has a strain of 1.5% in the direction of the short surface lattice vector and of 2.6% in the perpendicular direction, considering the theoretical value of the Pd-Pd distance (2.796 Å) and the theoretical C-C distance (1.42 Å). Upon relaxation, the graphene buckles resulting in a height difference of 1.2 Å between the highest and the lowest C atom. For comparison, suspended graphene structures may display height differences up to 1 nm [43]. The average edge energy of a zig-zag edge and of an armchair edge of graphene adsorbed on Pd(100) have been calculated by means of a (7×4) cell with an adsorbed nanoribbon [44, 45]. (7×4) and (6×4) surface cells have been employed for the zig-zag and armchair edges, respectively. The edge energy amounts to 0.53 eV/Å for the zig-zag edge, clearly lower than that for an isolated nanoribbon (2.03 eV/Å). For the armchair edge a value of 0.62 eV/Å has been found, higher than for the zig-zag edge. A complete graphene layer adsorbed on Pd(100) has a formation energy of 0.16 eV/C atom with respect to the clean surface and bulk graphite. A hexagonal form with only zig-zag edges has been assumed for the patch, and half of the distance between two opposite edges of the hexagon has been taken as the radius. With the system *1surf1subsub* on Pd(100) (see Tab. 3 and Fig. 3(d)) as reference, we obtain a critical radius of ∼5 nm for the growth of graphene patches (Fig. 4). This value shows that, in the first stages of carbon deposition, carbon might well dissolve into the metal. It is thus probable that, under the experimental conditions, considerable amounts of carbon might get into the metal before graphene formation becomes viable.

To corroborate this point, we have also calculated the barriers for diffusion of carbon at the Pd(100) surface and from a surface site to a subsurface site. For the surface diffusion, two possible diffusion pathways have been considered: in the first pathway, the carbon atom is moving from one hollow site to the next one via the connecting bridge site at the surface, while a diffusion through a subsurface tetrahedral position has been considered for the second pathway. Surprisingly, the barrier for the second path is lower (1.66 vs 2.00 eV), implying that the surface diffusion actually takes place through subsurface positions. An even lower barrier of 0.96 eV is found for a carbon atom to reach an octahedral site in the subsurface position. Nevertheless, all these barriers are relatively high in view that the catalytic processes take place at room temperature. Yet, the relatively high barrier might be the reason why an incubation time of several minutes is observed for the hydrogenation reaction to become selective (see Fig. 1 in the Supporting Information of Ref. [11]). Moreover, both the energies of graphene nucleation and diffusion barriers suggest that, at low carbon coverage, dissolution into the Pd bulk is preferred over graphite nucleation in the initial stages of carbon deposition.

A further property of C atoms adsorbed at Pd surfaces is that the effective interaction between them is repulsive, as it can be seen from the analysis of low-energy carbon configurations (Tab.

3 and Fig. 3). In the systems with 2 C atoms, for each surface the configuration with the lowest energy is that with the highest C-C distance. As a result, in the most favorable configurations one of the 2 C atoms lies well below the surface. The effective repulsion between adsorbed C atoms might be crucial in preventing the formation of C-C bonds, and therefore might be the main hindrance to the nucleation of graphite patches.

3.5 Selectivity of the hydrogenation reaction

It is widely believed that bulk-dissolved hydrogen is responsible for the total hydrogenation reaction [11]. The results presented in the previous sections suggest that Pd_6C is present under reaction conditions. We have therefore investigated the diffusion of hydrogen in metallic palladium and in Pd_6C. At room temperature, the main diffusion mechanism of hydrogen in palladium is thermal hopping, whereas quantum tunneling becomes dominant below 120 K [46]. Moreover, in both diffusion mechanisms the transmission probability over a barrier has a strong dependence on the energy barrier, so that calculation of these barriers is relevant regardless of the actual diffusion mechanism. DFT without zero-point energies yields a very flat potential energy landscape for hydrogen in fcc palladium: the energy difference between the stable octahedral site and the tetrahedral site is just 0.05 eV, of the same order of magnitude as the thermal energy of one particle at room temperature. A NEB calculation for the barrier between two neighboring octahedral sites gives an estimate for the barrier of only 0.13 eV. This is in agreement with the fact that hydrogen diffuses very easily through palladium, so easily that this metal is even used as a filter to purify hydrogen gas. On the contrary, in Pd_6C the energy barrier between two neighbouring octahedral sites amounts to 0.37 eV, and hydrogen diffusion is hindered. We suspect that the reason for this effect is the disruption of the perfect Pd lattice; this implies that different kinds of impurities could lead to a similar effect. Indeed, it has been noted that gallium doping has a similar effect as carbon deposition on the selectivity of a palladium catalyst for the partial hydrogenation of alkynes [47]. In principle, beside the disruption of the Pd lattice, a role might be played by the electronic structure of the defect, for example through localized charge. However, it should be noted that the system is metallic also in presence of carbon and hydrogen. Therefore charges that might be present at the defect site are completely screened at long distances. At short distances, an interplay of chemical and electrostatic effects might be responsible for the effective C-H attraction observed.

A second element pointing to a higher selectivity of Pd_6C towards alkenes is given by adsorption energies of etyhne and ethene. The adsorption energies of ethyne and ethene on Pd(111) are -2.04 eV (Tab. 1) and -0.92 eV, respectively. On the $Pd_6C(0001)$ surface, which corresponds to the (111) surface in terms of the lattice vectors of fcc-Pd, the adsorption energies are -1.53 eV and -0.68 eV. The lower adsorption energies imply a shorter residence time for a molecule at the surface, and thus a lower reaction probability. This might favour partial hydrogenation over total hydrogenation.

4 Summary and conclusions

We have investigated the incorporation of carbon into a Pd catalysts by the means of density functional theory. We have found a bulk carbide Pd_6C phase with a $(\sqrt{3}\times\sqrt{3}\times6)$ cell with respect to the fcc lattice of Pd. This compound consists of Pd-octahedra with one C atom at the center, where every Pd atom is coordinated to one and only one C atom. The phase has a formation energy of 0.23 eV/C atom and yields core level shifts of 0.66-0.70 eV for the Pd 3d states, in agreement with the peak observed in XPS spectra. Although graphite is the thermodynamically stable phase, carbon dissolution into the metal is possible, because the large critical radius for graphene nucleation (on Pd(100): $\sim$5 nm) delays the formation of the stable graphite phase at the surface. The calculations show that hydrogen diffusion is hindered in Pd_6C in comparison to metallic Pd. Since bulk-dissolved hydrogen diffusing to the surface is thought to be the species responsible for the total hydrogenation of alkynes, these results could explain why the reaction becomes selective in presence of Pd_6C.

Acknowledgments

This work was financially supported by the FWF under the project "Nanoscience on surfaces". The authors would like to thank R. Schlögl for fruitful discussions.

References

[1] A. N. R. Bos, E. S. Bootsma, F. Foeth, H. W. J. Sleyster, and K. R. Westerterp, Chem. Eng. Process. 32, 53 (1993).

[2] N. S. Schbib, M. A. Garcia, C. E. Gigola, and A. F. Errazu, Ind. Eng. Chem. Res. 35, 1496 (1996).

[3] J. H. Kang, E. W. Shin, W. J. Kim, J. D. Park, and S. H. Moon, Catal. Today 63, 183 (2000).

[4] N. A. Khan, S. Shaikhutdinov, and H.-J. Freund, Catal. Lett. 108, 159 (2006).

[5] G. C. Battiston, L. Dalloro, and G. R. Tauszik, Appl. Catal. 2, 1 (1982).

[6] A. Mamedov, S. Al-Wahabi, A. Al-Alwan, Patent WO 2006/105799A2.

[7] J. Wood, M. J. Alldrick, J. M. Winterbottom, E. H. Stitt, and S. Bailey, Catal. Today 128, 52 (2007).

[8] P. G. Menon, Chem. Rev. 94, 1021 (1994).

[9] H. Lindlar, Helv. Chim. Acta 35, 446 (1952).

[10] A. B. McEwen, M. J. Guttieri, W. F. Maier, R. M. Laine, and Y. Shvo, J. Org. Chem. 48, 4436 (1983).

[11] D. Teschner, J. Borsodi, A. Wootsch, Z. Revay, M. Hävecker, A. Knop-Gericke, S. D. Jackson, and R. Schlögl, Science 320, 86 (2008).

[12] D. Teschner, E. Vass, M. Hävecker, S. Zafeiratos, P. Schnörch, H. Sauer, A. Knop-Gericke, R. Schlögl, M. Chamam, A. Wootsch, A. S. Canning, J. J. Gamman, S. D. Jackson, J. McGregor, and L. F. Gladden, J. Catal. 242, 26 (2006).

[13] D. Teschner, Z. Revay, J. Borsodi, M. Hävecker, A. Knop-Gericke, R. Schlögl, D. Milroy, S. D. Jackson, D. Torres, and P. Sautet, Angew. Chem. Int. Ed. 47, 9274 (2008).

[14] P. G. Menon, J. Mol. Catal. 59, 207 (1990).

[15] P. Albers, J. Pietsch, and S. F. Parker, J. Mol. Catal. A: Chem. 173, 275 (2001).

[16] M. Larsson, J. Jansson, and S. Asplund, J. Catal. 178, 49 (1998).

[17] M. Larsson, J. Jansson, and S. Asplund, J. Catal. 162, 365 (1996).

[18] P. Albers, S. Bösing, G. Prescher, K. Seibold, D. K. Ross, and S. F. Parker, Appl. Catal. A: Gen. 187, 233 (1999).

[19] P. Albers, K. Seibold, G. Prescher, and H. Müller, Appl. Catal. A: Gen. 176, 135 (1999).

[20] I. Y. Ahn, J. H. Lee, S. S. Kum, and S. H. Moon, Catal. Today 123, 151 (2007).

[21] J. P. Perdew, K. Burke, and M. Ernzerhof, Phys. Rev. Lett. 77, 3865 (1996).

[22] P. E. Blöchl, Phys. Rev. B 50, 17953 (1994).

[23] G. Kresse and D. Joubert, Phys. Rev. B 59, 1758 (1999).

[24] G. Kresse and J. Hafner, Phys. Rev. B **47**, 558 (1993).

[25] L. Köhler and G. Kresse, Phys. Rev. B 70, 165405 (2004).

[26] G. Mills, H. Jonsson, and G. K. Schenter, Surf. Sci. 324, 305 (1995).

[27] C. Matsumoto, Y. Kim, T. Okawa, and Y. Sainoo, M. Kawai, Surf. Sci. 587, 19 (2005).

[28] P. A. Sheth, M. Neurock, and C. M. Smith, J. Phys. Chem. B 107, 2009 (2003).

[29] F. Mittendorfer, C. Thomazeau, P. Raybaud, and H. Toulhoat, J. Phys. Chem. B 107, 12287 (2003).

[30] C. G. P. M. Bernardo and J. A. N. F. Gomes, J. Mol. Struct.-Teochem 629, 251 (2003).

[31] B. Hammer, Y. Morikawa, and J. K. Nørskov, Phys. Rev. Lett. 76, 2141 (1996).

[32] S. B. Ziemecki, G. A. Jones, D. G. Swartzfager, R. L. Harlow, and J. Faber, J. Am. Chem. Soc. 107, 4547 (1985).

[33] J. A. McCaulley, Phys. Rev. B 47, 4873 (1993).

[34] T. Yamamoto, M. Adachi, K. Kawabata, K. Kimura, and H. W. Hahn, Appl. Phys. Lett. 63, 3020 (1993).

[35] N. Krishnankutty and M. A. Vannice, J. Catal. 155, 312 (1995).

[36] B. Wang, H. Q. Wang, Y. Q. Li, S. Y. Zhang, and J. G. Hou, Mater. Res. Bull. 35, 551 (2000).

[37] S. Ono, T. Kikegawa, and Y. Ohishi, Solid State Commun. 133, 55 (2005).

[38] E. Gregoryanz, C. Sanloup, M. Somayazulu, J. Badro, G. Fiquet, H.-K. Mao, and R. J. Hemley, Nature Mater. 3, 294 (2004).

[39] A. R. Oganov and C. W. Glass, J. Chem. Phys. 124, 244704 (2006).

[40] G. Trimarchi, A. J. Freeman, and A. Zunger, Phys. Rev. B 80, 092101 (2009).

[41] A. Baraldi, L. Bianchettin, E. Vesselli, S. de Gironcoli, S. Lizzit, L. Petaccia, G. Zampieri, G. Comelli, and R. Rosei, New J. Phys. 9, 143 (2007).

[42] R. J. Wolf, K. A. Mansour, M. W. Lee, and J. R. Ray, Phys. Rev. B 46, 8027 (1992).

[43] J. C. Meyer, A. K. Geim, M. I. Katsnelson, K. S. Novoselov, T. J. Booth, and S. Roth, Nature 446, 60 (2007).

[44] C. Berger, Z. M. Song, X. B. Li, X. S. Wu, N. Brown, C. Naud, D. Mayou, T. B. Li, J. Hass, A. N. Marchenkov, E. H. Conrad, P. N. First, and W. A. de Heer, Science 312, 1191 (2006).

[45] F. Cervantes-Sodi, G. Csanyi, S. Piscanec, and A. C. Ferrari, Phys. Rev. B 77, 165427 (2008).

[46] H. Okuyama, W. Siga, N. Takagi, M. Nishijima, and T. Aruga, Surf. Sci. 401, 344 (1998).

[47] J. Osswald, K. Kovnir, M. Armbrüster, R. Giedigleit, R. E. Jentoft, U. Wild, Y. Grin, and R. Schlögl, J. Catal. 258, 219 (2008).

Table 1: Formation energies for various surface phases of ethyne. For Pd(111) a $(2\sqrt{3} \times \sqrt{3})$ surface cell has been employed, for Pd(100) a (4×2). The adsorption energies are reported with respect to an isolated ethyne molecule in the gas phase and the bare surface. CH adsorbs in the hollow site on Pd(100) and in the HCP-hollow on Pd(111).

Structure	E_{ads} (eV)	Structure	E_{ads} (eV)
Pd(111)			
$C_2H_2^{ads}$	−2.04	C_2^{ads} + $2H^{ads}$	−0.37
$2CH^{ads}$	−1.72	$2C^{ads}$ + $2H^{ads}$	−1.44
Pd(100)			
$C_2H_2^{ads}$	−2.75	C_2^{ads} + $2H^{ads}$	−1.37
$2CH^{ads}$	−2.81	$2C^{ads}$ + $2H^{ads}$	−3.61

Table 2: Formation energies for various Pd-C phases, calculated with respect to bulk palladium and graphite. Pd_3C has the same structure as Pd_2C with one C vacancy per unit cell. Pd_4C is the structure with one C atom in the conventional cell of metallic Pd.

structure	ΔH_f (eV/C atom)	Structure	ΔH_f (eV/C atom)
Pd_2C	4.44	Pd_3C	3.6
Pd_4C	1.16	$Pd_{32}C$	0.92
$Pd_{32}C_2$	0.77	Rutile	1.19
Rocksalt	2.83	Zincblende	3.10
Sc_2C	1.60	Ti_2C	1.84
Cr_3C_2	2.38	$Cr_{23}C_6$	1.94
Mn_5C_2	1.03	Mn_7C_3	0.93
Fe_2C	1.54	Fe_3C	1.65
Co_2C	1.65	Co_3C	1.66
Ni_3C	1.20	Y_2C	3.24
Nb_2C	1.63	Mo_2C	1.19
Ta_2C	1.63	W_2C	1.19

Table 3: Formation energies of various surface phases with adsorbed-dissolved carbon. The formation energies are calculated with respect to the bare Pd surface and to graphite. For Pd(111) a $(\sqrt{3} \times \sqrt{3})$ surface cell has been employed, for Pd(100) a (2×2) surface cell. The position "subsub" lies one layer lower than the "sub" (subsurface) position (see Fig. 3).

structure	ΔH_f (eV/C atom)	Structure	ΔH_f (eV/C atom)
Pd(111)			
1surf	0.93	1sub	0.18
1sub1surf	1.35	2sub	1.14
1sub1subsub	0.53	1sub1subsubsub	0.27
Pd(100)			
1surf	−0.25	1sub	0.32
2surf	0.36	1surf1sub	0.27
2sub	0.90	1surf1subsub	0.20
2surf1sub	0.63	1surf1sub1subsub	0.47

Table 4: Core level shifts of the 3d states of Pd, for Pd(111) with dissolved carbon. *1sub* refers to a $(\sqrt{3} \times \sqrt{3})$ cell with one C atom in a subsurface octahedral site; *1sub1subsubsub* refers to one more C atom in an octahedral site two layers below (see text and Fig. 3(a-b)). The first label of the atoms refers to the layer number (1=surface atom); the second is an atom index in the layer.

1sub	CLS (eV)		CLS (eV)		CLS (eV)
$Pd_{1,1-3}$	+0.46	$Pd_{2,1-3}$	+0.59		
$Pd_{3,1}$	−0.05	$Pd_{3,2}$	+0.00	$Pd_{3,3}$	+0.00
1sub1subsubsub	CLS (eV)		CLS (eV)		CLS (eV)
$Pd_{1,1}$	+0.48	$Pd_{1,2}$	+0.47	$Pd_{1,3}$	+0.48
$Pd_{2,1}$	+0.64	$Pd_{2,2}$	+0.59	$Pd_{2,3}$	+0.64
$Pd_{3,1}$	+0.60	$Pd_{3,2}$	+0.65	$Pd_{3,3}$	+0.65

Table 5: Core level shifts of the 3d states of Pd, for Pd(100) with dissolved carbon or hydrogen. *1surf1subsub* refers to a (2×2) cell with one C atom in a hollow site at the surface, and one in an octahedral site two layers below; *1surf1sub1subsub* refers to one more C atom in a subsurface site (see text and Fig. 3(c-f)). The first label of the atoms refers to the layer number (1=surface atom); the second is an atom index in the layer.

With C	CLS (eV)		CLS (eV)		CLS (eV)
1surf1subsub					
$Pd_{1,1-4}$	+0.49	$Pd_{2,1}$	+0.57	$Pd_{2,2}$	−0.25
$Pd_{2,3}$	+0.71	$Pd_{2,4}$	−0.25	$Pd_{3,1-4}$	+0.75
1surf1sub1subsub					
$Pd_{1,1}$	+0.62	$Pd_{1,2}$	+0.73	$Pd_{1,3}$	+1.02
$Pd_{1,4}$	+0.62	$Pd_{2,1}$	+1.10	$Pd_{2,2}$	+0.74
$Pd_{2,3}$	+1.10	$Pd_{2,4}$	+0.74	$Pd_{3,1}$	+0.91
$Pd_{3,2}$	+0.79	$Pd_{3,3}$	+1.15	$Pd_{3,4}$	+0.79
$Pd_{4,1}$	+0.93	$Pd_{4,2}$	−0.07		
With H					
$Pd_{1,1}$	−0.57	$Pd_{1,2}$	−0.14	$Pd_{1,3}$	−0.14
$Pd_{1,2}$	−0.08	$Pd_{2,1}$	+0.06	$Pd_{2,2}$	+0.27
$Pd_{2,3}$	+0.17	$Pd_{2,4}$	+0.18	$Pd_{3,1}$	+0.33
$Pd_{3,2}$	+0.09	$Pd_{3,3}$	+0.09	$Pd_{3,4}$	+0.34

Table 6: Core level shifts of the 3d states of Pd, for Pd(100) with dissolved carbon and hydrogen. *1surf1subsub* refers to a (2×2) cell with one C atom in a hollow site at the surface, and one in an octahedral site two layers below; *1surf1sub1subsub* refers to one more C atom in a subsurface site (see text and Fig. 3(c-f)). The first label of the atoms refers to the layer number (1=surface atom); the second is an atom index in the layer.

With C and H	CLS (eV)		CLS (eV)		CLS (eV)
1surf					
$Pd_{1,1}$	+0.83	$Pd_{1,2}$	+0.81	$Pd_{1,3}$	+0.81
$Pd_{1,4}$	+0.82	$Pd_{2,1}$	+0.19	$Pd_{2,2}$	+0.11
$Pd_{2,3}$	+0.10	$Pd_{2,4}$	+0.75	$Pd_{3,1}$	+0.40
$Pd_{3,2}$	+0.07				
1surf1subsub					
$Pd_{1,1}$	+0.96	$Pd_{1,2}$	+0.89	$Pd_{1,3}$	+0.90
$Pd_{1,4}$	+0.96	$Pd_{2,1}$	+0.81	$Pd_{2,2}$	+0.21
$Pd_{2,3}$	+0.06	$Pd_{2,4}$	+0.96	$Pd_{3,1}$	+1.26
$Pd_{3,2}$	+1.08	$Pd_{3,3}$	+1.09	$Pd_{3,4}$	+1.26

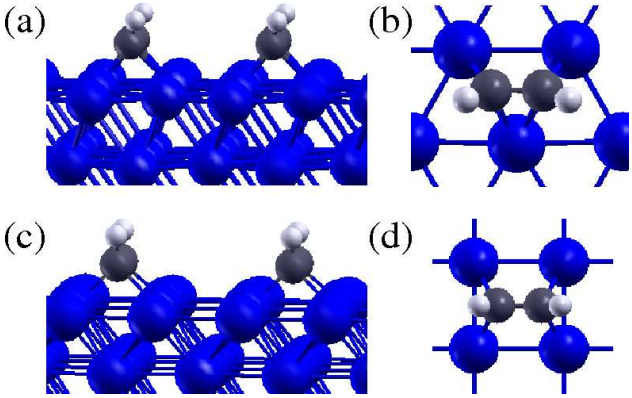

Figure 1: Ethyne adsorption on Pd(111): (a) view from the side and (b) from above. (c) and (d) are the corresponding views for Pd(100). Blue balls - Pd atoms; grey balls - carbon atoms; white balls - hydrogen atoms.

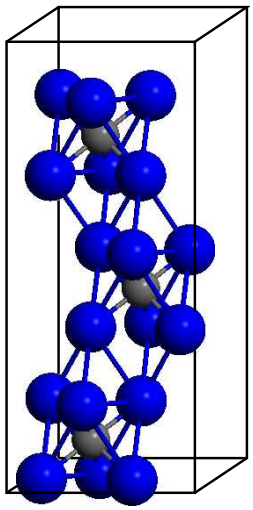

Figure 2: Crystal structure of Pd_6C. The elementary cell corresponds to a $(\sqrt{3} \times \sqrt{3} \times 6)$ cell of fcc palladium, and contains three octahedra each consisting of 6 Pd atoms with one carbon atom at the center. Blue balls - Pd atoms; grey balls - carbon atoms.

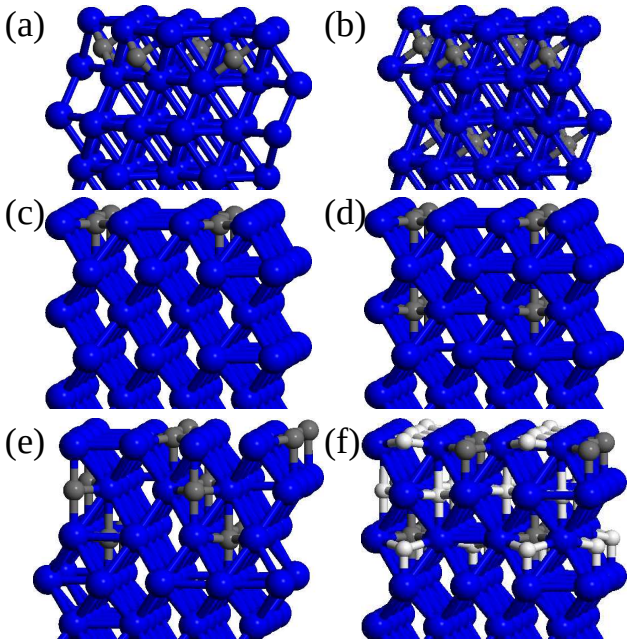

Figure 3: Models of carbon dissolved in palladium surfaces: (a) carbon in a subsurface position on Pd(111) (*1sub*); (b) carbon in a subsurface position and one layer further below on Pd(111) (*1sub1subsubsub*); (c) carbon at the surface on Pd(100) (*1surf*); (d) carbon at the surface and two layers below on Pd(100) (*1surf1subsub*); (e) carbon at the surface, at a subsurface position and one layer below on Pd(100) (*1surf1sub1subsub*); (f) same as (d) with additional dissolved hydrogen. Blue balls - Pd atoms; grey balls - carbon atoms; white balls - hydrogen atoms.

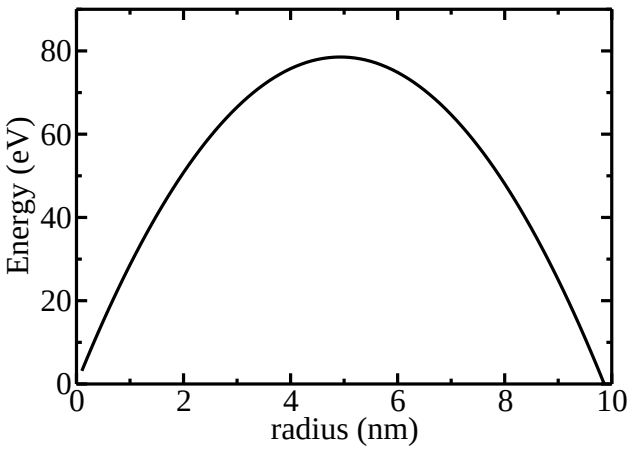

Figure 4: Calculated energy of a graphene patch supported on Pd(100) as a function of the patch radius. The reference energy is fixed at the *1surf1subsub* structure of dissolved C in Pd(100) (see Fig. 3).